

Article

Effect of Alkaline Treatment on the Catalytic Performance of ZSM-5 Catalyst in Pyridine and Picolines Synthesis

Fang Jin, Ye Tian, and Yongdan Li

Ind. Eng. Chem. Res., **2009**, 48 (4), 1873-1879 • DOI: 10.1021/ie8014457 • Publication Date (Web): 08 January 2009

Downloaded from <http://pubs.acs.org> on March 2, 2009

More About This Article

Additional resources and features associated with this article are available within the HTML version:

- Supporting Information
- Access to high resolution figures
- Links to articles and content related to this article
- Copyright permission to reproduce figures and/or text from this article

[View the Full Text HTML](#)



ACS Publications
High quality. High impact.

Effect of Alkaline Treatment on the Catalytic Performance of ZSM-5 Catalyst in Pyridine and Picolines Synthesis

Fang Jin,^{†,*} Ye Tian,[†] and Yongdan Li^{*,†}

Tianjin Key Laboratory of Applied Catalysis Science and Technology and State Key Laboratory for Chemical Engineering (Tianjin University), School of Chemical Engineering, Tianjin University, Tianjin 300072, People's Republic of China, and Key Laboratory for Green Chemical Process of Ministry of Education, School of Chemical and Pharmaceutical Engineering, Wuhan Institute of Technology, Wuhan 430073, People's Republic of China

An alkaline treatment is employed for tailoring a commercial H-ZSM-5 to produce a catalyst for the synthesis of pyridine and picolines. The most significant consequence of the alkaline treatment was desilication. However, it is accompanied by extraction of aluminum and formation of extra-framework aluminum (Al_{ef}) and amorphous alumina. Slit-shaped intracrystalline mesopores and macropores form. Because of the decrease in the Si/Al ratio in the zeolite framework and the formation of Al_{ef} and amorphous alumina, the number of strong acid sites decreases and that of weak acid sites increases. The ratio of Lewis acids to Brønsted acids (L/B) also increases. We note that the induced hierarchical pores and the change of acid strength distribution increase the stability of the catalyst, and the increased L/B causes an increase in the initial yield and comparative selectivity for pyridine and a decrease in those properties for 3-picoline. Coking leads to a gradual deactivation and affects product selectivity.

1. Introduction

Chichibabin condensation of formaldehyde, acetaldehyde, and ammonia has been explored extensively for the vapor-phase synthesis of mixed pyridine bases (i.e., pyridine and picolines), which are the key intermediates in the production of pharmaceutical, agricultural, and other fine chemicals. There is growing interest for H-ZSM-5 to be used as the catalyst for the Chichibabin condensation. The intrinsic acidity and shape selectivity of pentasil structure cause it to possess greater pyridine base selectivity than other acid catalysts, such as amorphous silica–alumina, H-A, H-X, H-Y, and H-mordenite.^{1–3} H-ZSM-5 has tunable acidity, three-dimensional porosity, high thermal stability, and the capability to stabilize active metal clusters, so that its modification to fit Chichibabin condensation may develop a more-efficient catalyst.^{1,2,4,5} Nevertheless, the intracrystalline diffusion limitation and strong acidity in its micropores frequently result in heavy coking and deactivation.^{4,6}

The diffusion limitation in micropores can be minimized by enlarging pore size and the acidity of the zeolite can be monitored by direct assembly and post-synthesis modification techniques.^{7–11} Alkaline treatment, which is referenced as desilication in the literature,^{12–17} has been introduced as an effective approach for creating extra pores and modifying the acidity in high-silicon zeolites, such as H-ZSM-5.

In this work, we investigated the effect of the alkaline treatment of a commercial small-crystal-size H-ZSM-5, to improve its stability and activity in the Chichibabin condensation reaction.

2. Experimental Section

2.1. Catalyst Samples. The original ZSM-5 zeolite was provided by the Nanlian Institute of Sinopec Jinling Petrochemical Corporation. The sample was calcined at 823 K for 5 h to convert it to H-form, following the guidance of the manufacturer. This sample is designated as H-ZSM-P.

For alkaline treatment, H-ZSM-P was stirred in a slurry that was composed of 1 g of zeolite in 30 mL of 0.2 M NaOH solution at 338 K for 0.5 h. The slurry was then cooled with an ice bath and filtrated. The filtration cake was washed with deionized water until a pH value of 7 was reached, and then it was dried in air at 383 K. After alkaline treatment, the Na-form sample was obtained. It was ion-exchanged with 1 g of zeolite in 50 mL of 1 M NH_4NO_3 solution, and with stirring at 298 K in a flask for 8 h. The material was filtrated and washed with deionized water, then dried at 383 K. The ion-exchange and wash–filtration–drying procedure was repeated 3 times. The H-form, which is called H-ZSM-At, was obtained via calcination at 823 K for 5 h.

A commercial spherical catalyst with a diameter of ~ 5 mm and a H-ZSM-P/ γ - Al_2O_3 ratio of 7:3 (γ - Al_2O_3 is the binder used for extrusion) was also provided by the same company. The sample was crushed, calcined at 823 K for 5 h, and was converted directly to H-form. This sample is referenced as H-ZSM-B.

2.2. Characterization. Powder X-ray diffraction (XRD) was performed using a Rigaku D/max 2500 v/pc automatic diffractometer. Scanning electron microscopy (SEM) micrographs were obtained using a Hitachi X-650 microscope. The attached energy-dispersive X-ray analysis (EDX) equipment was used to analyze the bulk Si/Al ratio. Solid-state nuclear magnetic resonance (²⁷Al and ²⁹Si NMR) spectra were collected with a Varian Infinity Plus 300 WB spectrometer. ²⁹Si spectra were recorded at 59.6 MHz, with a pulse width of 10 μ s, a pulse delay of 50 s, and a spinning rate of 4 kHz.

* To whom correspondence should be addressed. Tel.: +86-22-27405613. Fax: +86-22-27405243. E-mail address: ydli@tju.edu.cn.

[†] Tianjin Key Laboratory of Applied Catalysis Science and Technology and State Key Laboratory for Chemical Engineering (Tianjin University), School of Chemical Engineering, Tianjin University.

^{*} Key Laboratory for Green Chemical Process of Ministry of Education, School of Chemical and Pharmaceutical Engineering, Wuhan Institute of Technology.

^{27}Al spectra were obtained at 78.1 MHz, with a pulse width of 0.6 μs , a pulse delay of 20 s, and a spinning rate of 4 kHz.

N_2 adsorption and desorption isotherms were measured at 77 K on a Quantachrome NOVA-2000 gas sorption analyzer after vacuum pretreatment at 473 K for 8 h. Total specific surface areas (S_{BET}) were calculated using the Brunauer–Emmett–Teller (BET) method,¹⁸ and the total pore volume (V_{total}) was evaluated from N_2 uptake at a relative N_2 pressure of 0.99. The t -plot was employed to evaluate the volume of micropores (V_{microp}) and the total surface area (S_{surf}) of mesopores, macropores, and external crystal surface.¹⁹ The pore size distribution (PSD) was determined using the Barrett–Joyner–Halenda (BJH) method,²⁰ which was applied to the adsorption branches of the isotherms. High-resolution transmission electron microscopy (HRTEM) images were observed using a Philips TECNAI G² F20 electron microscope.

Temperature-programmed desorption, using ammonia (NH_3 -TPD), was conducted with a quartz reactor and a 200-mg sample with a particle size of 0.18–0.28 mm at atmospheric pressure with a thermal conductivity detector (TCD) device. The system was quenched at 673 K for 1 h in a helium flow of 40 mL/min (STP). After cooling to 373 K, NH_3 was introduced with a pulsed injection with the helium flow until saturation. The sample was quenched again at 373 K for 2 h, to remove the excess NH_3 . Desorption was then performed under the same helium flow, with a ramp of 8 K/min to 973 K.

The Fourier transform infrared (FTIR) spectra of H-ZSM-5-adsorbed pyridine were collected in transmission mode, using a Bruker Vector 22 spectrometer. The samples were ground into fine powders and pressed into very thin self-supporting wafers with an optical diameter of 16 mm. The disks were mounted in a quartz infrared (IR) cell that was equipped with a CaF_2 window and a vacuum system. Prior to adsorption, the samples were pretreated in situ at 673 K for 1.5 h under evacuation, and then were cooled to 398 K when pyridine vapor was introduced into the cell for 0.5 h by vaporizing the pyridine in an evaporator at room temperature. The physically adsorbed pyridine was removed by evacuation for 1 h, then the sample was heated under vacuum at 473 K for 2 h and a spectrum was recorded. The areas under the IR bands were calculated with OPUS software.

The thermogravimetry (TG) curves of the catalysts after reaction were measured with a Pyris 6 TG/DTG thermal analyzer. For these experiments, 20-mg samples were used and the thermograms were recorded under a flow of air at a rate 10 mL/min (STP) with a ramp of 10 K/min from 313 K to 1173 K.

2.3. Catalytic Reaction. The reaction was conducted in a stainless steel tubular reactor with a diameter of 10 mm at atmospheric pressure and 723 K, using 1.5 g of catalyst with a particle size of 0.18–0.28 mm, which was crushed and sieved from tablets formed without any binder at 35.5 MPa. A 60% acetaldehyde aqueous solution, and a 40% formaldehyde aqueous solution were mixed and vaporized in a preheater at 523 K. The stream was then mixed with gas-phase ammonia and hydrogen to comprise a $\text{C}_2\text{H}_4\text{O}:\text{CH}_2\text{O}:\text{NH}_3:\text{H}_2\text{O}:\text{H}_2$ molar ratio of 2:3:10:17:5. The gas hourly space velocity (GHSV) was 3131 h^{-1} . The liquid product was collected using an ice trap and then analyzed with an Agilent 6890 GC gas chromatograph that was equipped with a HP-5 column. The yields of pyridine and 3-picoline were used as a measure of catalytic activity, which is calculated as

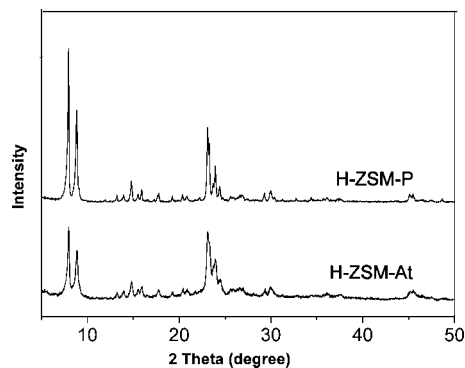


Figure 1. XRD patterns of (A) H-ZSM-P and (B) H-ZSM-At.

$$\text{yield (\%)} = \frac{\text{total C atoms in product}}{\text{total C atoms in feed}} \times 100\%$$

The ratio between the yield of pyridine and that of 3-picoline (P/3P) indicates the selectivity, as discussed later.

3. Results

3.1. Structure and Composition. H-ZSM-P and H-ZSM-At display (Figure 1) XRD peaks at similar positions. This indicates that the H-ZSM-5 crystal structure was not destroyed during the treatment. However, the XRD pattern of H-ZSM-At has broader peaks with lower intensities than that of H-ZSM-P, indicating that the crystallinity or the nominal crystal size was effectively reduced.

The ^{29}Si NMR spectra of the samples are displayed in Figure 2A. The silicon atoms in the zeolite framework are tetrahedrally coordinated, resulting in five different silicon environments, denoted as $\text{Si}(n\text{Al})$, where n corresponds to the number of Al atoms in the second coordination sphere ($n = 0, 1, 2, 3, \text{ or } 4$). In H-ZSM-5, only two types of $\text{Si}(n\text{Al})$ (i.e., $\text{Si}(0\text{Al})$ and $\text{Si}(1\text{Al})$) are usually observed, because of its high Si/Al ratio.²¹ The chemical shift of $\text{Si}(1\text{Al})$ is ~ 106 ppm, and that of $\text{Si}(0\text{Al})$ is ~ 112 ppm.²¹ In this work, the areas of these two peaks were calculated with deconvolution of the spectrum using the Gaussian method. The framework Si/Al ratio in zeolites ($(\text{Si}/\text{Al})_{\text{frame}}$) is calculated with the equations

$$\text{Si/Al} = \frac{S_{\text{(total)}}}{0.25S_{\text{Si}(1\text{Al})}}$$

and

$$S_{\text{total}} = S_{\text{Si}(0\text{Al})} + S_{\text{Si}(1\text{Al})}$$

where $S_{\text{Si}(0\text{Al})}$ and $S_{\text{Si}(1\text{Al})}$ are the areas of $\text{Si}(0\text{Al})$ and $\text{Si}(1\text{Al})$ signal peaks, respectively.^{22,23} The results are shown in Table 1. After alkaline treatment, the $(\text{Si}/\text{Al})_{\text{frame}}$ value decreased. Table 1 gives also the Si/Al ratios measured by EDX ($(\text{Si}/\text{Al})_{\text{Bulk}}$) and NMR ($(\text{Si}/\text{Al})_{\text{Frame}}$). $(\text{Si}/\text{Al})_{\text{Bulk}}$ is the global average, because the technique detects a depth of $\sim 1 \mu\text{m}$ and the crystal size of the sample here is ~ 500 – 700 nm. The alkaline treatment leads to an obvious decrease of $(\text{Si}/\text{Al})_{\text{Bulk}}$.

The ^{27}Al NMR spectra of the samples are displayed in Figure 2B. The signal at ~ 50 ppm is ascribed to the tetrahedral framework aluminum (Al_f).^{23,24} The resonance at ~ 0 ppm is due to the octahedral extraframework aluminum (Al_ef) or amorphous Al_2O_3 (Al_a).^{25–27} To estimate the relative amount of tetrahedral Al_f and octahedral Al, areas of the two peaks were calculated with deconvolution of the spectrum using the Gaussian method.^{27,28} These data are also listed in Table 1. Both 50 ppm and 0 ppm peaks are shown in the spectrum of the

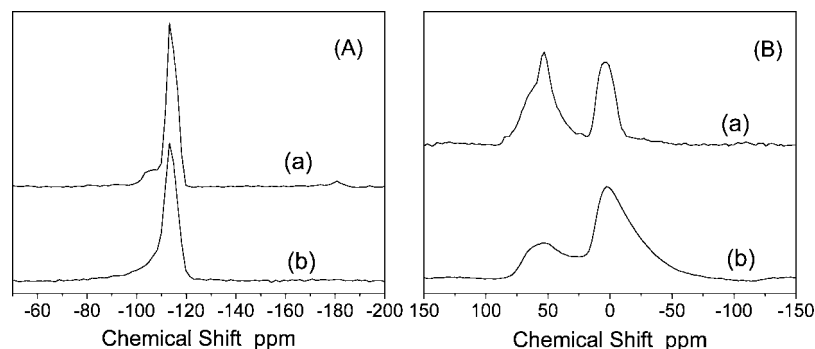


Figure 2. (A) ^{29}Si NMR spectra of H-ZSM-P (spectrum a) and H-ZSM-At (spectrum b). (B) ^{27}Al NMR spectra of H-ZSM-P (spectrum a) and H-ZSM-At (spectrum b).

Table 1. ^{27}Al NMR and ^{29}Si NMR Peak Areas Corresponding to Different Chemical Shifts and the Si/Al Ratios Measured by Two Techniques

sample	$(\text{Si}/\text{Al})_{\text{Bulk}}^a$	Area of the ^{27}Al NMR Peak			Area of the ^{29}Si NMR Peak		$(\text{Si}/\text{Al})_{\text{Frame}}$
		$S_{50 \text{ ppm}} (\times 10^{-9})$	$S_{0 \text{ ppm}} (\times 10^{-9})$	$S_{50 \text{ ppm}}/S_{0 \text{ ppm}}$	$S_{-106 \text{ ppm}} (\times 10^{-8})$	$S_{-112 \text{ ppm}} (\times 10^{-8})$	
H-ZSM-P	2.84	1.35	0.91	1.5	0.22	1.71	35
H-ZSM-At	1.72	0.63	1.18	0.5	0.76	1.42	12

^a Measured via energy-dispersive X-ray analysis (EDX).

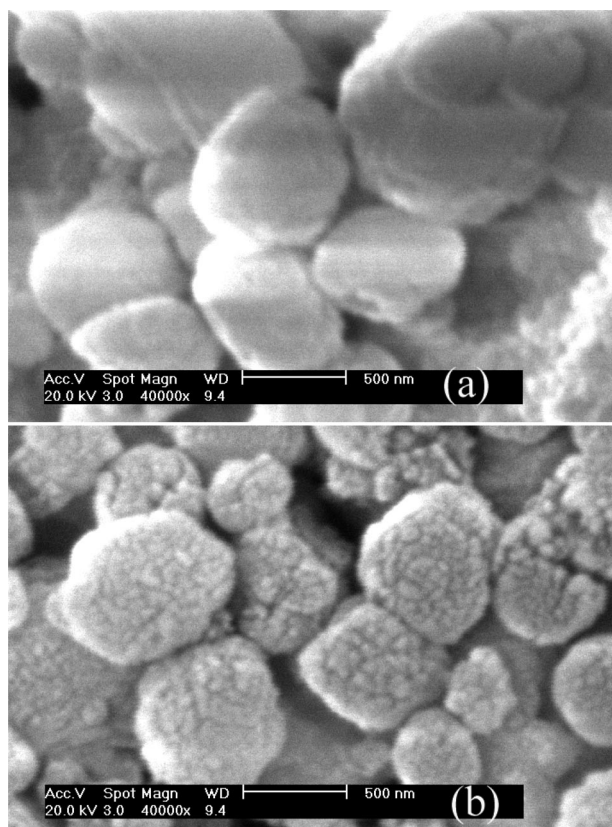


Figure 3. Scanning electron microscopy (SEM) micrographs of (a) H-ZSM-P and (b) H-ZSM-At.

parent sample. This result demonstrates that the parent sample contains not only Al_f but also $\text{Al}_{ef} + \text{Al}_a$. After desilication, the $\text{Al}_{ef} + \text{Al}_a$ peak increased and that of Al_f decreased. The ratio of peak area at 50 ppm to that at 0 ppm decreased from 1.5 to 0.5. This is an indication of simultaneous dealumination.

3.2. Morphology and Texture. The SEM micrographs of the samples are given in Figure 3. H-ZSM-P has a smooth surface and a crystal size of 500–700 nm. After the alkaline treatment, the morphology changed dramatically. Grooves and voids appeared on the surface of crystal and asteroidal cracks formed at the center of some crystals. Some of the crystals were

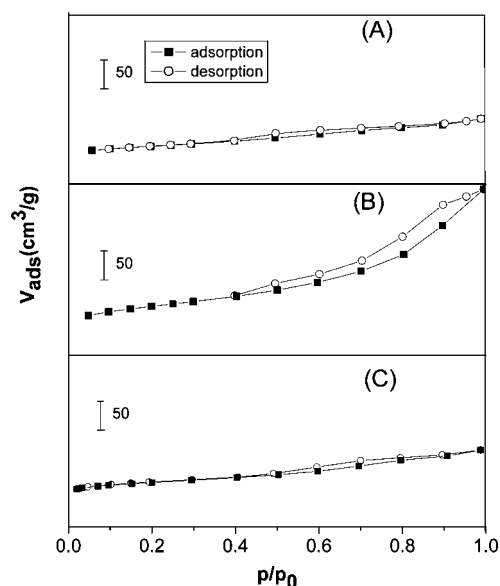


Figure 4. (■) N_2 adsorption and (○) N_2 desorption isotherms at 77 K: (A) H-ZSM-P, (B) H-ZSM-At, and (C) H-ZSM-B.

fractured. Nevertheless, the overall crystal size does not change much during treatment.

The nitrogen adsorption–desorption isotherms are depicted in Figure 4. The isotherm of H-ZSM-P exhibits a Type I curve, because of its microporous nature. A very small H2-type hysteresis loop that is present probably suggests the existence of mesopores in H-ZSM-P. After alkaline treatment, the isotherm was transformed from Type I to Type IV. The uptake of N_2 at higher relative pressures was enhanced, indicating the increased contribution of mesopores. The shape of the hysteresis loop became Type H3, suggesting modification of the pores to a slit-shaped morphology.²⁹ The isotherms of H-ZSM-B are similar to those of H-ZSM-P.

The pore-size distribution (PSD) curves that were calculated with the BJH model, using the data of the adsorption branch, are illustrated in Figure 5. H-ZSM-P has pore diameters of 1–11 nm, whereas the curve of H-ZSM-At develops a broad peak of 1–100 nm. The curve of H-ZSM-B is similar to that of H-ZSM-P. Table 2 summarizes the S_{BET} , V_{total} , V_{microp} , mesopore volume

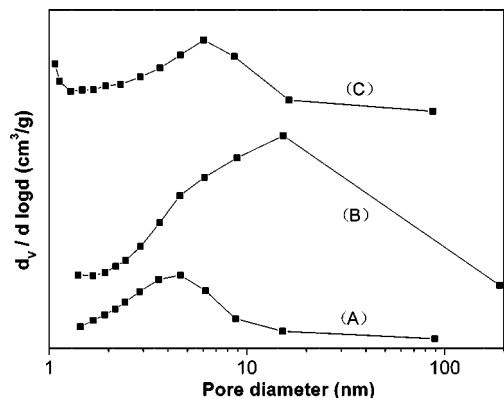


Figure 5. Barret–Joyner–Halenda (BJH) pore-size distribution (PSD) curves, derived from the adsorption branches: (A) H-ZSM-P, (B) H-ZSM-At, and (C) H-ZSM-B.

(V_{mesop}), and S_{surf} information that was obtained. The BET model for the calculating of micropores can be reasonably used for comparison purposes.¹⁶ The data in Table 2 show that, after alkaline treatment, the S_{BET} and V_{total} values each increased. The V_{mesop} value increased 150%, whereas the value of V_{microp} decreased 32%. The HRTEM images of H-ZSM-P and H-ZSM-At are illustrated in Figure 6. After the desilication, fringes of the crystal were corroded, while the micropore structure remained.

3.3. Acidity. Figure 7 illustrates the NH_3 -TPD curves for two samples. Both have two peaks, corresponding to two types of acid sites (i.e., the weak sites associate with the TPD peak at ~ 500 – 600 K, and the strong sites relate to the peak at ~ 650 – 750 K). The result indicates that the acid strength distribution has changed, because of the treatment. The total number of acid sites has increased, while the number of strong sites decreased and the number of weak sites increased.

Figure 8 represents the variation of the IR bands after the adsorption of pyridine in the 1425 – 1575 cm^{-1} region. The band at ~ 1450 cm^{-1} , arising from the C–C stretch of a coordinatively bonded pyridine complex, indicates the presence of Lewis acid (L) sites. The ~ 1540 cm^{-1} band is attributed to the C–C stretching vibration of the pyridinium ion and has been used to identify the Brønsted acid (B) sites. Another band at ~ 1490 cm^{-1} is attributed to the pyridine species, which interact with the two types of acid sites.³⁰ The areas under the IR bands at ~ 1450 and ~ 1540 cm^{-1} contain information regarding the relative ratio of the L and B sites (L/B). This ratio was measured to be 6.9 prior to the treatment and 13.2 after the treatment.

3.4. Catalytic Performance. Figures 9A and 9B plot the curves of the yield of pyridine and 3-picoline as a function of the time-on-stream (TOS). The initial pyridine yield of H-ZSM-P was slightly lower than that of H-ZSM-At and H-ZSM-B, whereas the initial 3-picoline yield of H-ZSM-P was higher than that of H-ZSM-At and H-ZSM-B. After 8 h of reaction, the pyridine and picoline yield of H-ZSM-P decreased $\sim 10\%$ and $\sim 28\%$, respectively. After ~ 6.5 h of reaction, the pyridine and picoline yield of H-ZSM-B decreased $\sim 10\%$ and $\sim 31\%$, respectively. However, after 8 h of reaction, the pyridine and picoline yields of H-ZSM-At fluctuated in the range of 6% and 4%, respectively. These results indicated that the stability of H-ZSM-At was better than that of H-ZSM-P and H-ZSM-B for the synthesis of pyridine and 3-picoline.

Figure 9C depicts the P/3P ratios as a function of TOS. The initial P/3P ratio of H-ZSM-P was less than that of H-ZSM-At and H-ZSM-B, whereas the initial P/3P ratio of H-ZSM-At and H-ZSM-B were similar. The P/3P ratio of H-ZSM-P and

H-ZSM-B increased as the TOS increased, while that of H-ZSM-At was stable.

3.5. Used Catalyst. The thermograms of two used catalysts after 8 h reaction are shown in Figure 10. The weight loss of H-ZSM-At was much less than that of H-ZSM-P. The texture data of the two used samples are also summarized in Table 2. The S_{BET} , V_{total} , V_{microp} , V_{mesop} , and S_{surf} data for H-ZSM-P decreased by 67%, 60%, 65%, 57%, and 65%, respectively, after reaction, whereas those of H-ZSM-At decreased by 41%, 31%, 28%, 31%, and 42%, respectively.

4. Discussion

4.1. Phase Composition. The parent zeolite phase has a small crystal size (500–700 nm), which was verified by SEM imaging. This sample contains Al_{ef} and Al_{a} , which were detected by nuclear magnetic resonance (NMR) but were essentially XRD-amorphous. Kasture et al.²⁶ and Borzatta et al.³¹ found that ZSM-5 zeolite bounded with Al_2O_3 has peak positions similar to those of pure ZSM-5. After the alkaline treatment, the XRD pattern confirms preservation of the original crystal ordering of H-ZSM-5, but with a much smaller nominal crystal size or a reduced crystallinity, as the peaks were widened and weakened. However, the SEM images show no obvious apparent crystal size change, except for abundant cracks and flaws in the treated crystal.

The $(\text{Si}/\text{Al})_{\text{frame}}$ and $(\text{Si}/\text{Al})_{\text{Bulk}}$ ratios of H-ZSM-At are less than those of H-ZSM-P. Therefore, the major effect of alkaline treatment is desilication, although simultaneous dealumination happened.²⁷ ^{27}Al NMR data in Figure 2 and Table 1 reveal that the amount of Al_{f} decreases, while that of Al_{ef} and Al_{a} increases significantly. This result indicates that part of the Al_{f} transforms to Al_{ef} and Al_{a} during the treatment. It is likely that the alkaline corrosion preferentially starts at the silicon position, and the aluminum in the detached part was finally transformed from a tetrahedral coordination to an octahedral coordination. This is consistent with the findings of Groen et al.¹⁷ and Lietz et al.¹²

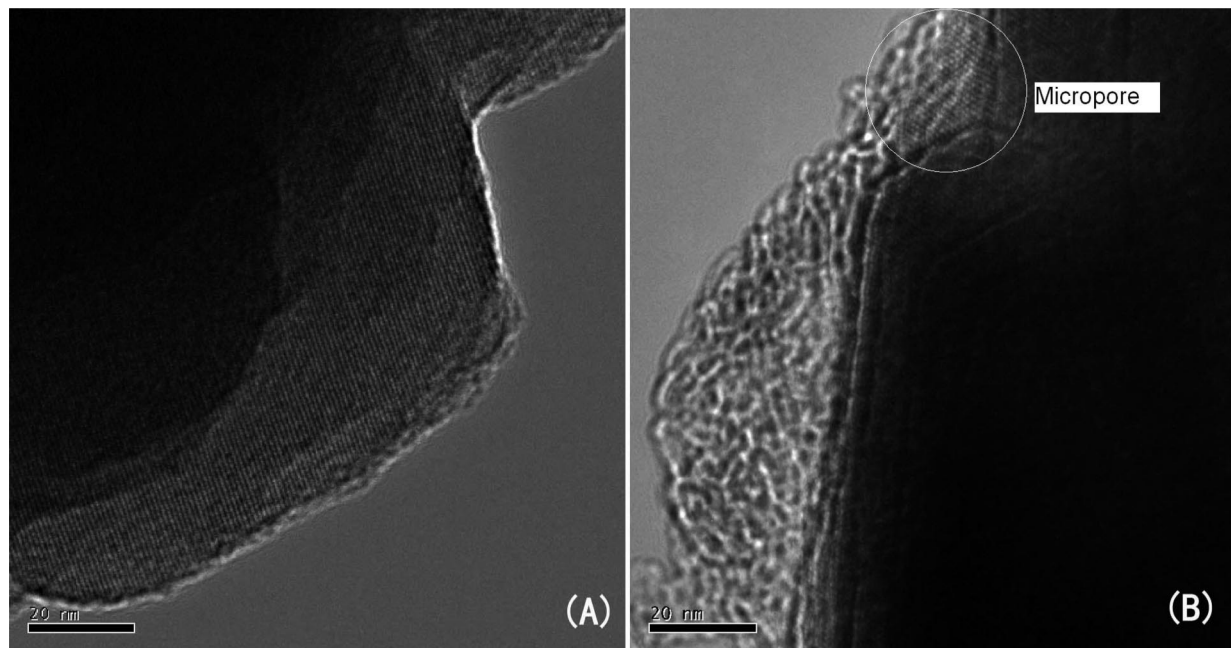
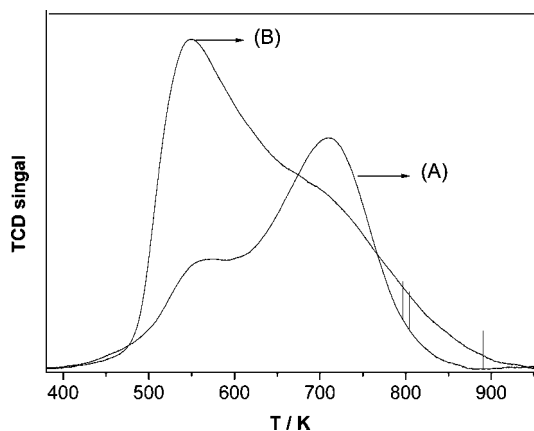
4.2. Texture and Morphology. The S_{BET} and V_{microp} values of H-ZSM-P are less than that of the typical ZSM-5 sample, because they contain amorphous alumina. A few intercrystallite mesopores exist in H-ZSM-P, which results in a slightly larger value of V_{total} than that in regular ZSM-5, as the data show in Table 2. Some mesopores may exist at the interface between the ZSM-5 and alumina crystals, as reported in the literature.^{13,32,33} The shape of the hysteresis loop of the isotherms changes after alkaline treatment. Groen et al.^{34,35} proposed that adsorption branch data are better for mesopore calculation with the BJH model than desorption data of the isotherm. The PSD curves here are calculated based on the adsorption data. The result shows that the pore diameters changed from 1–11 nm to 1–100 nm during desilication. Apparently, here, alkaline treatment is very effective for creating mesopores and macropores in H-ZSM-5.

The V_{microp} value remains high in H-ZSM-At, which indicates that micropores are only partially destroyed during the treatment. As for the origin of mesopores and macropores that formed during alkaline treatment, there exist several arguments. Ogura et al.¹⁵ proposed that the mesopores stemmed from intercrystalline porosity that formed from the removal of amorphous SiO_2 between twin crystals. Eiemek et al.¹³ found that “holes” formed on the crystal surface. Groen et al.¹⁶ assumed the formation of intracrystalline mesopores, based on the existence of large hollows within crystals.³⁶ As seen in Figure 3, we observed the formation of asteroidal flaws. This is similar to the intracrystalline mesopores observed by Groen et al.³⁷ However,

Table 2. Textural Properties of Different Samples

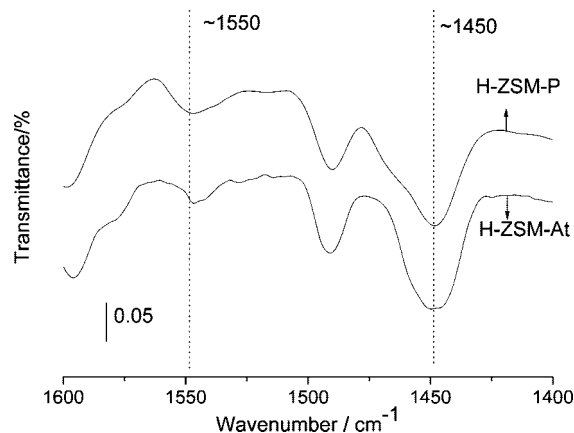
sample	S_{BET} (m ² /g)	V_{total} (cm ³ /g)	V_{microp} (cm ³ /g)	V_{mesop}^a (cm ³ /g)	S_{surf} (m ² /g)
H-ZSM-P	227	0.18	0.06	0.12	109
H-ZSM-At	302	0.45	0.04	0.41	217
used H-ZSM-P	75	0.07	0.02	0.05	38
used H-ZSM-At	177	0.31	0.03	0.28	126

$$^a V_{\text{mesop}} = V_{\text{total}} - V_{\text{micro}}$$

**Figure 6.** High-resolution transmission electron microscopy (HRTEM) micrographs of (A) H-ZSM-P and (B) H-ZSM-At.**Figure 7.** NH₃-TPD spectra of (A) H-ZSM-P and (B) H-ZSM-At.

some works suggested that mesopores formed at the interface between ZSM-5 and alumina crystals.^{13,32,33} Here, the PSD of H-ZSM-B is similar to that of H-ZSM-P and indicates no interface pores in the range of 10–100 nm. The HRTEM images further prove that the regular micropore structure persists after the treatment.

4.3. Acidity. After alkaline treatment, the results of a decreased amount of strong acid sites and an increased amount of weak acid sites are in agreement with those reported by Ogura et al.¹⁵ The alkaline treatment caused a decrease of the (Si/Al)_{frame} ratio, which, in turn, leads to an increase of the amount of weak acid sites and a decrease of the amount of strong acid sites. This is likely related to the formation of Al_{ef} and Al_a and the reduction of Al_f. Kim et al.³⁸ determined that mixing Na(H)-ZSM-5 with γ -Al₂O₃ resulted in a higher intensity of the NH₃-

**Figure 8.** Fourier transform infrared (FTIR) spectra obtained after the adsorption of pyridine over H-ZSM-P and H-ZSM-At at 473 K.

TPD peak in the low-temperature range and a lower intensity of the peak in the high-temperature range.

The treatment dislodged Al_f, resulting in the decrease of the amount of B sites in the zeolite framework. Some of the formed Al_{ef} and Al_a may act as L sites.^{38,39} It is observed that the treatment increased the L/B ratio.

4.4. Catalytic Performance. H-ZSM-At has a longer lifetime in the reaction than H-ZSM-P. Three groups of authors^{40–42} found that zeolite mixed with binder (i.e., kaolinite, Al₂O₃, and silica) had a lower deactivation rate than zeolite itself for *n*-heptane cracking, propylene oligomerization, and propane aromatization reactions. Fougier et al.⁴⁰ proposed that a binder such as Al₂O₃ acts as a coke sink and protects the zeolite. Here, H-ZSM-B, which is composed of H-ZSM-P and Al₂O₃, has a

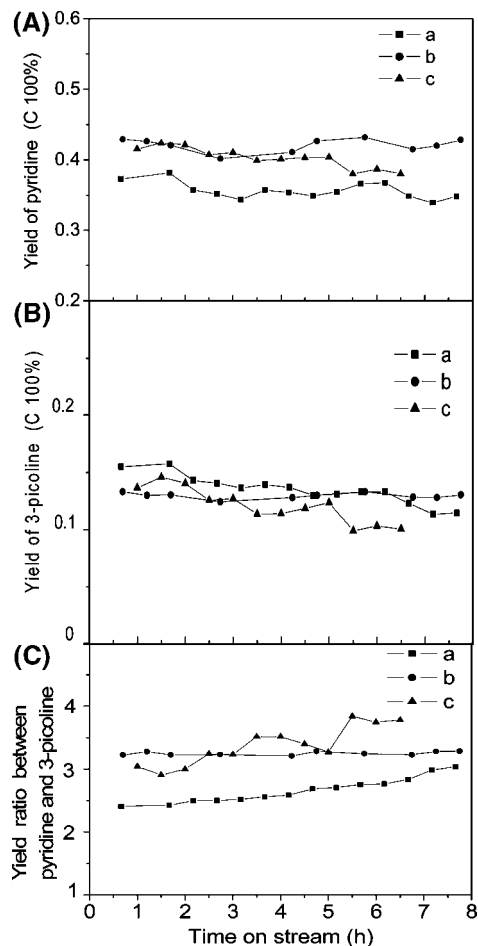


Figure 9. Yields of pyridine and 3-picoline, and their ratio, versus the time-on-stream (TOS): (A) yield of pyridine, (B) yield of 3-picoline, and (C) the pyridine/3-picoline yield ratio. (Legend: H-ZSM-P (spectrum a, ●), H-ZSM-At (spectrum b, ■), and H-ZSM-B (spectrum c, ▲).)

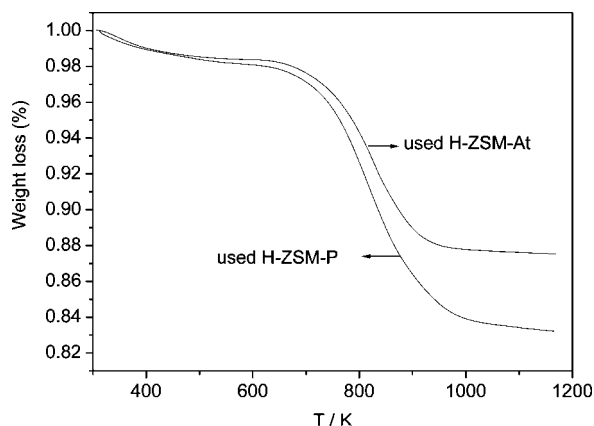
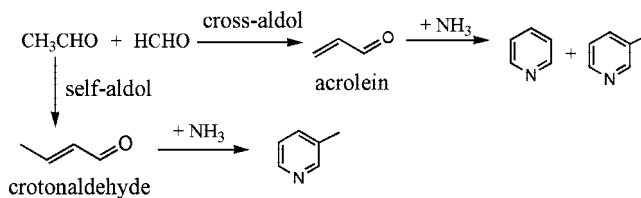


Figure 10. TG curves of used H-ZSM-P and H-ZSM-At after 8 h of TOS.

performance similar to that of H-ZSM-P. In this reaction, the coke sink effect of Al_2O_3 seemingly is not obvious.

The deactivation of ZSM-5 in the reaction is attributed to the formation of coke, which covers the acid sites and blocks the micropore of zeolites. The alkaline treatment increased the total amount of acid sites at the expense of acid strength. Changes in the acid strength distribution may lead to slower coking. Meanwhile, a large number of secondary mesopores and macropores were introduced. This may weaken the diffusion limitation of the intermediates and products in the micropores,

Scheme 1. Simplified Mechanism of Chichibabin Condensation for Pyridine and 3-Picoline Synthesis from Formaldehyde, Acetaldehyde, and Ammonia



as well the moderate pore coverage effect of coke and its precursors. Data in Figure 10 prove that the carbonaceous species deposited on H-ZSM-At were much less than those on H-ZSM-P. The data in Table 2 demonstrate that the decreases of the percentages of S_{BET} , V_{total} , V_{microp} , V_{mesop} , and S_{surf} of H-ZSM-At are much lower than those of H-ZSM-P, which indicated a moderated surface coverage and pore blockage effect of the carbonaceous species for the treated catalyst.

Both B and L acid sites participated in the Chichibabin reaction but may involve different mechanisms.² Singh et al.⁴³ proposed a mechanism for the synthesis of pyridine bases from formaldehyde, acetaldehyde, and ammonia, in which the cross-aldol condensation of formaldehyde and acetaldehyde occurs and generates an intermediate (acrolein), and the self-aldol condensation of acetaldehyde occurs and generates another intermediate (crotonaldehyde). Consequently, acrolein reacts with ammonia and generates both pyridine and 3-picoline, while crotonaldehyde reacts with ammonia and generates only 3-picoline. The mechanism can be described by Scheme 1. Dumitriu et al.⁴⁴ investigated the aldol condensation of formaldehyde and acetaldehyde over MFI zeolites. They found that, on B sites, acetaldehyde is more favorable than formaldehyde in forming a cation and reacting with the enol form of acetaldehyde, because acetaldehyde has higher electronic density at the O atom than formaldehyde; therefore, crotonaldehyde is favored over acrolein. They postulated also that L sites favor acrolein because formaldehyde is easier to activate on L sites and cross-condensation is enhanced to the same extent. After alkaline treatment, the L/B ratio increased, and, according to the aforementioned mechanism, acrolein should be enhanced while crotonaldehyde should be depressed. This leads to an increase in the P/3P ratio. Our experimental results are consistent with such reasoning, that the initial pyridine yield of H-ZSM-At is higher and the initial 3-picoline yield of H-ZSM-At is lower than those of H-ZSM-P.

As the TOS increased, the P/3P increased. This reflects the coke-induced change in selectivity. The amounts of the deposited carbonaceous species increased as the TOS increased. This induces a gradual pore blockage. The larger intermediate (crotonaldehyde) and 3-picoline then are not favored anymore over the smaller intermediate (acrolein) and pyridine. Because the H-ZSM-At sample has an improved pore system, the pore blockage of this sample is less severe than that of the untreated sample and the P/3P ratio is more stable with the TOS than the untreated sample.

5. Conclusions

The most significant consequence of alkaline treatment of ZSM-5 is desilication, although dealumination also occurs simultaneously. After the treatment, both the $(\text{Si}/\text{Al})_{\text{Frame}}$ and $(\text{Si}/\text{Al})_{\text{Bulk}}$ ratios decrease. Some of the Al_f is extracted, and both Al_a and Al_{ef} form. The treated sample retains the ZSM-5 crystalline structure and regular micropores. A large amount of

cracks and flaws are introduced into the crystals and a large amount of slit-shaped mesopores and macropores are created. Pores in the 10–100 nm range form, resulting mostly from intracrystallite flaws. After treatment, the pores, acid strength distribution, and L/B ratio are also modified. The increase in the number of weak acid sites, the decrease of the strong acid sites, and the increase of L/B ratio are all attributed to the decrease in the $(\text{Si}/\text{Al})_{\text{frame}}$ ratio and the formation of Al_a . These modifications effectively improve the stability of the catalyst. This is ascribed to the change of the acid strength distribution and the introduced secondary pores, which, in turn, depress coke formation and diminish the blockage effect of carbonaceous species. The initial pyridine yield and selectivity are slightly enhanced after the treatment, whereas the initial 3-picoline yield and selectivity are depressed after the treatment. These are all attributed to the increase in the L/B ratio from alkaline treatment, which enhances the formation of the intermediate acrolein and favors the generation of pyridine, and depresses the formation of intermediate crotonaldehyde and the generation of 3-picoline. An increase of pyridine selectivity and a decrease of 3-picoline selectivity, relative to the increasing TOS, are observed during the reaction for the H-ZSM-P sample, and the treated sample exhibits the most stable P/P3 ratio. This can be explained within the context of the same mechanism with the effect of coke-induced change in selectivity.

Acknowledgment

This work is supported by the Natural Science Foundation of China (under Contract No. 20425619). The work has also been supported by the Program of Introducing Talents to the University Disciplines (under File No. B06006), and the Program for Changjiang Scholars and Innovative Research Teams in Universities (under File No. IRT 0641) and the Youths Science Foundation of Wuhan Institute of Technology (under File No. Q200901).

Literature Cited

- (1) Shimizu, S.; Abe, N.; Iguchi, A.; Dohba, M.; Sato, H.; Hirose, K. *Microporous Mesoporous Mater.* **1998**, *21*, 447.
- (2) Shimizu, S.; Abe, N.; Iguchi, A.; Sato, H. *Catal. Surv. Jpn.* **1998**, *2*, 71.
- (3) Calvin, J. R.; Davis, R. D.; Mcafee, C. H. *Appl. Catal., A* **2005**, *285*, 1.
- (4) Liu, Y. M.; Yang, H. Q.; Jin, F.; Zhang, Y.; Li, Y. D. *Chem. Eng. J.* **2008**, *136*, 282.
- (5) Jin, F.; Cui, Y. G.; Li, Y. D. *Appl. Catal., A* **2008**, *350*, 71.
- (6) Angevene, P. J.; Chu, C. T. (Mobil Oil Corporation). U.S. Patent 5,395,940, 1995.
- (7) Janicke, M. T.; Landry, C. C.; Christiansen, S. C.; Birtalan, S.; Stucky, G. D.; Chmelka, B. F. *Chem. Mater.* **1999**, *11*, 1342.
- (8) Meng, X. C.; Wu, Y. X.; Li, Y. D. *J. Porous Mater.* **2006**, *13*, 365.
- (9) Liu, H. R.; Meng, X. C.; Zhao, D. S.; Li, Y. D. *Chem.—Eur. J.* **2008**, *14*, 424.
- (10) Zhang, H. J.; Li, Y. D. *Powder Technol.* **2008**, *183*, 73.
- (11) Zhang, H. J.; Meng, X. C.; Li, Y. D.; Lin, Y. S. *Ind. Eng. Chem. Res.* **2007**, *46*, 4186.
- (12) Lietz, G.; Schnabel, K. H.; Peuker, C.; Gross, T.; Storek, W.; Völter, J. *J. Catal.* **1994**, *148*, 562.
- (13) Eiemek, A.; Subotić, B.; Aiello, R.; Crea, F.; Nastro, A.; Tuoto, C.; Eiemek, A.; Subotić, B.; Sumit, I.; Tonejc, A.; Aiello, R.; Crea, F.; Nastro, A. *Microporous Mater.* **1995**, *4*, 159.
- (14) Le, T. S.; Le Van Mao, R. *Microporous Mesoporous Mater.* **2000**, *34*, 93.
- (15) Ogura, M.; Shinomiya, S.; Tateno, J.; Nara, Y.; Nomura, M.; Kikuchi, E.; Matsukata, M. *Appl. Catal., A* **2001**, *219*, 33.
- (16) Groen, J. C.; Peffer, L. A. A.; Moulijn, J. A.; Pérez-Ramírez, J. *Microporous Mesoporous Mater.* **2004**, *69*, 29.
- (17) Groen, J. C.; Peffer, L. A. A.; Moulijn, J. A.; Pérez-Ramírez, J. *Chem.—Eur. J.* **2005**, *11*, 4983.
- (18) Brunauer, S.; Emmett, P. H.; Teller, E. *J. Am. Chem. Soc.* **1938**, *60*, 309.
- (19) Lippens, B. C.; de Boer, J. H. *J. Catal.* **1965**, *4*, 319.
- (20) Barret, E. P.; Joyner, L. G.; Halenda, P. P. *J. Am. Chem. Soc.* **1951**, *73*, 373.
- (21) Engelhardt, G.; Fahlke, B.; Maegi, M.; Lippmaa, E. *Z. Phys. Chem. (Leipzig)* **1985**, *266*, 239.
- (22) Engelhardt, G.; Michel, D. *High-Resolution Solid-State NMR of Silicates and Zeolites*; Wiley: Chichester, U.K., 1987; p 205.
- (23) Fyfe, C. A.; Gobbi, G. C.; Kennedy, G. J. *J. Phys. Chem.* **1984**, *88*, 3248.
- (24) Sawa, M.; Niva, M.; Murakami, Y. *Zeolites* **1990**, *10*, 532.
- (25) Klinowski, J.; Thomas, J. M.; Fyfe, C. A.; Gobbi, G. C.; Hartman, J. S. *Inorg. Chem.* **1983**, *22*, 63.
- (26) Kasture, M. W.; Niphadkar, P. S.; Bokade, V. V.; Joshi, P. N. *Catal. Commun.* **2007**, *8*, 1003.
- (27) Zhang, Y. W.; Zhou, Y. M.; Qiu, A. D.; Wang, Y.; Xu, Y.; Wu, P. C. *Ind. Eng. Chem. Res.* **2006**, *45*, 2213.
- (28) Deng, F.; Yue, Y.; Ye, C. H. *J. Phys. Chem.* **1998**, *102*, 5252.
- (29) Gregg, S. J.; Sing, K. S. W. *Adsorption, Surface Area and Porosity*, 2nd Edition; Academic Press: London, 1982; pp 111–194.
- (30) Jin, F.; Li, Y. D. *Catal. Today* DOI: 10.1016/j.cattod.2008.06.007.
- (31) Borzatta, V.; Busca, G.; Poluzzi, E.; Rossetti, V.; Trombetta, M.; Vaccari, A. *Appl. Catal., A* **2004**, *257*, 85.
- (32) Le Van Mao, R. *Microporous Mesoporous Mater.* **1999**, *28*, 9.
- (33) Klint, D.; Bovin, J. O. *Mater. Res. Bull.* **1999**, *34*, 721.
- (34) Groen, J. C.; Peffer, L. A. A.; Pérez-Ramírez, J. *Microporous Mesoporous Mater.* **2003**, *60*, 1.
- (35) Groen, J. C.; Pérez-Ramírez, J. *Appl. Catal., A* **2004**, *268*, 121.
- (36) Groen, J. C.; Brouwer, S.; Peffer, L. A. A.; Ramírez, J. P. *Part. Part. Syst. Character.* **2006**, *23*, 101.
- (37) Groen, J. C.; Bach, T.; Ziese, U.; Paulaime-van Donk, A. M.; De Jong, K. P.; Moulijn, J. A.; Pérez-Ramírez, J. *J. Am. Chem. Soc.* **2005**, *127*, 10792.
- (38) Kim, S. D.; Baek, S. C.; Lee, Y. J.; Jun, K. W.; Kim, M. J.; Yoo, I. S. *Appl. Catal., A* **2006**, *309*, 139.
- (39) Motz, J. L.; Heinichen, H.; Hölderich, W. F. *Stud. Surf. Sci. Catal.* **1997**, *105*, 1053.
- (40) Fougerit, M. J.; Gnep, N. S.; Guisnet, M.; Amigues, P.; Duplan, J. L.; Hugues, F. *Stud. Surf. Sci. Catal.* **1994**, *84*, 1723.
- (41) Misk, M.; Joly, G.; Magnoux, P.; Guisnet, M.; Jullian, S. *Microporous Mesoporous Mater.* **2000**, *40*, 197.
- (42) Choudhary, V. R.; Devadas, P.; Kinage, A. K.; Guisnet, M. *Appl. Catal., A* **1997**, *162*, 223.
- (43) Singh, B.; Roy, S. K.; Sharma, K. P.; Goswami, T. K. *J. Chem. Technol. Biotechnol.* **1998**, *71*, 246.
- (44) Dumitriu, E.; Hulea, V.; Fecchet, I.; Aurous, A.; Lacaze, J. F.; Guimon, C. *Microporous Mesoporous Mater.* **2001**, *43*, 341.

Received for review September 25, 2008

Revised manuscript received November 16, 2008

Accepted December 2, 2008

IE8014457